X-Morf: a crash-separable quadrotor that morfs its X-geometry in flight

A Desbiez, F. Expert, M Boyron, J Diperi, S. Viollet, F. Ruffier

X-Morf: a crash-separable quadrotor that morfs its X-geometry in flight

A. Desbiez[1], F. Expert[1], M. Boyron[1], J. Diperi[1], S. Viollet[1] and F. Ruffier[1]

Abstract— **The X-Morf robot is a 380-g quadrotor consisting of two independent arms each carrying tandem rotors, forming an actuated scissor joint. The X-Morf robot is able to actively change in-flight its X-geometry by changing the angle between its two arms. The magnetic and electrical joint between the quadrotors arms makes them easily removable and resistant to crashes while providing the propellers with sufficient power and ensuring high quality signal transmission during flight. The dynamic model on which the X-Morf robot was based, was also used to design an adaptive controller. A Model Reference Adaptive Control (MRAC) law was implemented to deal with the uncertainties about the inertia and the center of mass due to the quadrotors reconfigurable architecture and for in-flight span-adapting purposes. The tests performed with the X-Morf robot showed that it is able to decrease and increase its span dynamically by up to 28.5% within 0.5s during flight while giving good stability and attitude tracking performances.**

I. INTRODUCTION

Future quadrotors should be able to fly through increasingly complex and cluttered environments (see [6]). Under these conditions, however, most quadrotors are liable to be blocked by narrow passages they cannot cross because of their large span. In cluttered environment, birds fold their wings when flying between branches or through a fairly small gaps (see [14]). The goshawk is particularly good at morphing its shape in order to pass through apertures of various shapes, for example (see https://www.youtube.com/watch?v=2CFckjfP-1E). There are various ways of coping with narrowness. The most obvious solution is to use a small quadrotor. Micro quadrotors such as the Flexboat UAV (e.g., www.flexbot.cc) have been recently developed, but since the payload has to be kept very low on these vehicles, it is still difficult to address real-life missions by detecting such gap on the basis of embedded vision. Another solution consists in implementing means of performing aggressive maneuvers such as those described in [10]. However, this strategy requires powerful UAVs equipped with means of precisely tracking a specific predetermined trajectory such as highly precise motion capture cameras system. Planes and helicopters with adaptable flight modes have been previously designed to improve these vehicles flight performances (see [5]). Rotor tilting devices enable aircraft to act like a helicopter during take-off, landing and hovering as well as to fly as fast as planes during long trajectories.

Another category of aerial vehicles with adaptable shapes is that of wing-morphing aircraft (see [11], [15], [4], [3]). Some of these aircraft are able to optimize their shape to perform multi-objective missions. They can squeeze through narrow apertures but only at high speeds, which makes them unsuitable for indoor observation tasks, where low flight speed or stationary flight is sometimes required. A foldable quadrotor was recently presented, however in [12], the four branches of the quadrotor was able to unfold itself in response to a certain amount of thrust to start its flight, but such maneuver is irreversible and the pocket-size aerial robot cannot change back its size in-flight. Classical multirotors are usually composed of arms set around a rigid frame housing most of the equipment required (the power supply, control board(s), etc.). A quadrotor can also take the form of two crossed arms forming an "X". The approach adopted here for varying the size of a UAV during flight consisted in varying the angle between the quadrotor's two arms, as illustrated in Fig. 1. The idea of developing an aerial vehicle with a dynamically variable span was therefore investigated: this solution is compatible with fairly large payloads and a wide range of flight modes. The present study focused on the problem of finely adjusting the quadrotors span. In this paper, we will first describe how the X-Morf robot was designed to be able to morph its shape during flight. So far to our knowledge, X-Morf is the first ever quadrotor that is able to change its X-geometry in flight. The corresponding dynamic model and the adaptive control strategy adopted are then presented. The last section gives the results of test flights showing the stability and maneuverability of this initial prototype.

II. THE X-MORF ROBOT

The X-Morf robot is a micro-quadrotor featuring two main innovations:

- its ability to finely control its X-geometry during flight;
- and the magnetic docking mechanism (see figures 2.D and 3) with which the upper arm is equipped, which facilitates their removal and their packing as well as prevents much of the damage if crashes occur.

The two arms of the aerial robot lying on different planes are connected together via an actuated scissor joint. The lower arm will be referred to here as the fixed arm, and the upper arm, as the movable arm. The X-Morf robot is presented in Fig. 2.A.

A. The variable-span mechanism

The mechanism driving the folding of the arms has to meet several constraints. The propellers high rotational speed generates a momentum, which tends to rotate the arms. The

*This research was supported by CNRS Institutes (Biological Science; Information Science; Engineering Science and Technology), the Aix-Marseille University and the Aix-Marseille Carnot Institute "STAR".

[1]A. Desbiez, F. Expert, M. Boyron, J. Diperi, S. Viollet and F. Ruffier are with Aix Marseille Univ, CNRS, ISM, Marseille, France franck.ruffier@univ-amu.fr

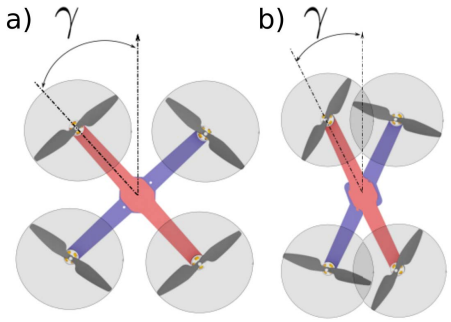

Fig. 1. X-geometry morphing principle. **A**. This figure shows a quadrotor with a classical 90deg-X configuration, which is also known as the scissor configuration. γ, the half of scissor-joint angle between its two arms is 45 deg. **B**. As the quadrotors two arms lie on two parallel planes only 4 cm apart, the propellers are liable to overlap. The X-Morf robot can change its span by up to 35% when the scissor-joint angle between its two arms is reduced from 90deg to 60deg.

actuator of the variable-span mechanism has to produce a sufficiently large torque for the angles of interest to be attained during flight. In addition, the scissor joint (see figure 2.C) has to allow power and signals to be transmitted between the movable arm and the fixed arm. The mechanism must have the friction as possible in order to keep the size and power requirements of the actuator to a minimum. And it must be as light-weight as possible to give the robot a suitably large operational range and make it crash-resistant and rigid enough to prevent the occurrence of vibration modes. The scissor joint mechanism (Fig. 2.A and 2.B) adopted in this initial prototype is inexpensive, robust and light-weight. With this joint, the upper arm can be rotated by up to 50 degrees. The joint was constructed with care in order to minimize the backlash, which is liable to cause a loss of control and the occurrence of vibration modes. The lower arm serving as a main frame, houses the robots main equipment and power supplies. Electrical connections between the main frame and the upper arm convey signals and power to the rotary arm via a hole provided in the scissor joint. The scissor joint is actuated by a servomotor (MKS DS95), which compensates for the drag torque generated by the propellers. A servomotor was used as the main actuator because it is lightweight and inexpensive and produces suitably high levels of torque and fast rotations. The servomotor also fits the quadrotors mechanical structure nicely. The torque required to rotate the arm was determined using an equation (1) published in a classical dynamic study.

$$C_m = I_{b_z}\dot{\gamma} + c_Q.\omega_2^2 + c_Q.\omega_4^2 \quad (1)$$

where I_{b_z} is the inertia of the upper arm on its vertical axis, $\dot{\gamma}$ is the rotation speed of the upper arm and $c_Q\omega_i^2$ is the drag momentum induced by the two propellers set on the upper arm. The servomotor was placed outside the frame, as shown in Fig.2.C. Although this might conceivably introduce a loss of balance, this disadvantage is offset by the fact that aligning the axis of the servomotor with the robots center of rotation would have given rise to fitting issues as well as weakening the robot mechanically. The joint between the servomotor and the cylindrical joint currently consists of a set of rods giving a gear ratio of 1 as well as a low backlash. The propellers are respectively defined by the points $O_{1,2,3,4}$, the center of the quadrotor is defined by O. The length of the half arm span is l. The frame is a direct orthonormal system oriented in the way that the X-Axis direction is always colinear to the angle bisector between the two arms.

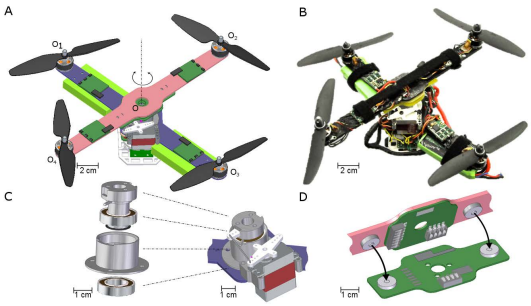

Fig. 2. The X-Morf robot. **A**. The X-Morf robot was first designed using CAD software. The lower (blue) arm carries most of electronics: two packs of batteries mounted below each propeller, the electronic boards placed under the central part of the lower arm, and the servomotor mounted at the top of the lower arm. The upper (pink) arm carries only the ESC. **B**. Photograph of the current X-Morf robot with a scissor-joint configuration. The architecture is the same as that obtained in the CAD model. The quadrotors two arms lie on two parallel planes only 4 cm apart. **C**. Exploded view of the scissor joint and its actuation mechanism. The scissor joint is composed of two aluminum parts, which can rotate with very little friction thanks to two plastic bearings. **D**. CAD model of the magnetic docking mechanism between the two arms. Two magnets provide the mechanical connections, whereas the three One Piece Power (OPP from Samtec Company) interface connectors provide the electronic connections. The final mechanism obtained is presented in Fig. 3.

B. A crash-separable upper-arm mechanism

The idea of having a removable upper arm arose from the need to make the quadrotor resilient to crashes. In the event of crashes, the impact is bound to disconnect the magnets and hence, the upper arm. This arrangement protects the frame, the propellers, the scissor joint and the servomotor from being damaged. It has been particularly useful during the adjustment of the X-Morf control law. The dockable arm can also be undocked manually for packing purposes. Providing the UAV with a removable arm makes for easy docking as well as facilitating the installation of the electrical connections required to carry power and signals to the upper arm. In order to protect the servomotor, the magnetic docking mechanism must release the upper arm in response to any impact but resist high-thrust maneuvers. The magnetic docking mechanism designed and constructed at our laboratory is presented in Fig. 2.D (see also Fig. 3). Two magnets are installed at the joint between two boards screwed to the top of the scissor joint and the upper arm. The magnetic joint holds these boards equipped with connectors together. As soon as a crash occurs, the magnets become separated and the electrical connection is cut, making the propellers stop immediately. Each of the connectors pins is able to transmit a maximum current of 2A, which is sufficiently strong for the PWM control signals but not for power transmission purposes. Four pins were therefore used to provide the power required by the two rotors on the upper arm. However, special attention had to be paid to the

positioning of the One Piece Power (OPP) interfaces in order to minimize the risk of electrical shortcut that would damage components during crashes.

Magnetic docking mechanism: Fig. 3 displays the resilient-shock mechatronical system conveying power and signals used onboard the X-Morf robot to make the flying robot resilient despite crashes. The system is composed of two part : one is glued to the upper arm (Fig. 3A) and the second is screwed to the upper part of the scissor joint (Fig. 3B). In case of a crash, the quadrotor "loses" its upper arm automatically canceling the applied torque on the servomotor and then preserving its integrity.

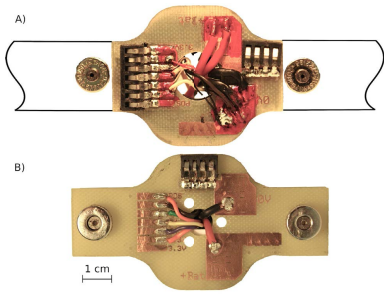

Fig. 3. Magnetic docking mechanism. The top and bottom photographs are the docking parts of the upper arms. **A)** Printed circuit board (PCB) and magnets directly glued to the upper arm. **B)** PCB equipped with complementary magnets screwed down to the upper part of the scissor joint.

C. Electronics

The X-Morf robot was mainly based on the X4-Mag quadrotor (see [9]): it is equipped with the same actuators, hardware and software. There are four different electronic boards: (i) A power management board fed by two battery packs placed below at the extremity of the lower arm. The wiring system was designed to facilitate the plugging and unplugging of the batteries. (ii) A low level Arduino NanoWii controller is equipped with a 6-axis Inertial Measurement Unit (IMU) composed of 3 rate-gyros and 3 accelerometers. The NanoWii board is able to control the attitude of a classical quadrotor, but in the present case, it was used to provide the X-Morf autopilot with inertial data. (iii) The Rotor Controller Board (RCB), a custom-made electrical board controlled the rotational speed of each rotor in the closed-loop mode. The electronic board consists of a 16-bit Microchip micro-controller with a clock frequency of 40MHz. The speeds of the rotors are closely controlled using a contactless tachometer, i.e., a small Hall effect sensor placed near each brushless motor, providing for each of the rotors, rotational speed measurement. A low-level controller of this kind increase the controllability of the X-Morf which is important to stabilize its attitude. (iv) A Gumstix Overo AirSTORM device that is a Computer-On-Module (COM) served as high level controller. A custom-made Linux operating system runs on this COM device. Thanks to the toolbox RT-MaG (http://www.gipsa-lab.fr/projet/RT-MaG/), the autopilot and controllers can be programmed using the toolbox provided with Matlab Simulink software. In addition, the board provides WIFI connections, which can be used to transmit data between the COM and a host computer. They can also be used to command the UAV from a ground station, as well as to tune parameters and monitor the state of the X-Morf robot during flight.

D. Characteristics

The X-Morf robot still belongs to the category of micro-quadrotors because of its low weight (380g) and its short (21cm) arm span. However, its reconfigurable architecture makes for some asymmetry on the X and Y-axes due to the presence of the servomotor, as well as on the Z-axis due to the position of the electrical boards below the propulsion center. Further asymmetry is introduced by the shift between the two propulsion centers on the lower and upper arms. These features can be deduced from the 3-D model using CAD software, but the data obtained in this way will not take into account some of the robots components, such as the wires, and the VICON markers used to locate the robot in our flying arena. The accuracy of the 3-D model in terms of the inertia and of the position of the center of mass is therefore subject to various uncertainties.

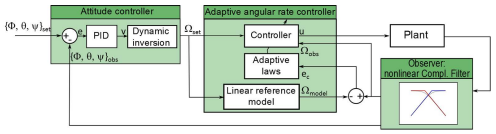

Fig. 4. PID-Attitude controller and Adaptive angular rate controller. The observer, which we have called the nonlinear complementary filter, was first developed in [8] and adapted to our previous Quaternion robot (see [9]). The outer loop is the attitude controller, which is composed of a classical PID combined with a dynamic inversion process taking into account the nonlinearities induced by (6). The inputs are the Euler angles set by the pilot; the outputs are the angular rates commanded, which are fed to the Adaptive angular rate control loop system.

III. Dynamics and Control

The half-angle γ (see Fig. 1) is bound to drastically affect the rotational dynamics of the quadrotor in several ways. Basically, it will greatly affect the inertial matrix $I(\gamma)$ as well as the thrust efficiency $D(\gamma)$. A study on the impact of the folding angle on the inertia was carried out in steady state using the CAD 3-D model. Closing the arm half-angle from 45 deg to 30 deg resulted in a decrease of about 35 % in the moment of inertia on the x and y axes. Such a large change in the inertia is bound to cause some problems in the low-level control of the X-Morf quadrotor. But before designing the X-Morf robots controllers, it was necessary to study its dynamics.

A. System dynamics

The control architecture of a quadrotor is composed of two loops:

- the inner loop, which is the angular rate loop, and
- the outer loop, which is the attitude loop.

The inputs to the inner loop are the angular rate setpoints Ω_{set}, and its outputs are the Euler angles describing the quadrotors attitude. The outer loop receives the attitude setpoints from the pilot and sends the angular rate setpoints to the inner loop. Each propeller exerts a thrust and a drag

(see equation (2)) along the upward (vertical) z-axis of the bodys fixed frame.

$$T_i = c_T(\gamma).\omega_i^2 \\ Q_i = c_Q(\gamma).\omega_i^2 \tag{2}$$

where c_T and c_Q are the thrust and drag coefficients, respectively. These coefficients depend on the folding half-angle γ resulting from the overlapping of the propellers. The thrust was measured experimentally depending on the folding angle, and the results were consistent with those presented in [7] and in [13]. Fig.5 shows the differences observed in the thrust in the case where the upper and lower propellers rotational planes were 5cm apart.

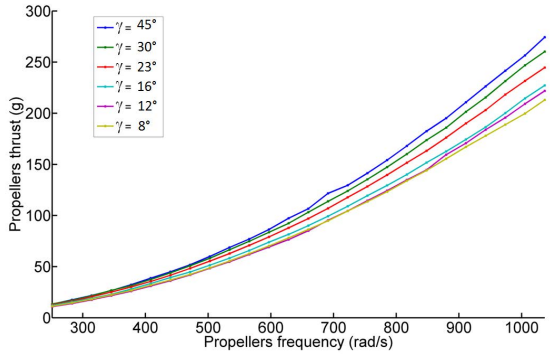

Fig. 5. Experimental results giving the evolution of the thrust at various rotational propeller speeds and arm angles γ.

These functions were approximated by a third order polynomial function (see equation (3)) to enhance the predictions:

$$c_T(\gamma) = -2.939.10^{-10}\gamma^3 + 4.01.10^{-8}\gamma^2 - 6.55.10^{-7}\gamma + 2.003.10^{-4} \tag{3}$$

For a fixed γ, the global moment applied at the center of mass can be expressed in the form of equation (4).

$$\tau = \overbrace{\begin{bmatrix} l.sin(\gamma).c_T & l.sin(\gamma).c_T & -l.sin(\gamma).c_T & -l.sin(\gamma).c_T \\ -l.cos(\gamma).c_T & l.cos(\gamma).c_T & l.cos(\gamma).c_T & -l.cos(\gamma).c_T \\ c_Q & -c_Q & c_Q & -c_Q \end{bmatrix}}^{\mathbf{D}(\gamma)} \begin{bmatrix} \omega_1^2 \\ \omega_2^2 \\ \omega_3^2 \\ \omega_4^2 \end{bmatrix} \tag{4}$$

Since the main torques exerted on the center of mass have been established, it is now possible to obtain the angular accelerations $\dot{\Omega}$:

$$\dot{\Omega} = \begin{bmatrix} \dot{p} & \dot{q} & \dot{r} \end{bmatrix}^T = \mathbf{I}(\gamma)^{-1}.(\tau - \Omega \times \mathbf{I}(\gamma).\Omega) \tag{5}$$

where $\mathbf{I}(\gamma)$ is the inertia expressed as a function of the folding half-angle γ.
The attitude angle rate in the inertial frames can be derived from the angular rate in the robot frame (see equation (6)).

$$\begin{bmatrix} \dot{\phi} \\ \dot{\theta} \\ \dot{\psi} \end{bmatrix} = \begin{bmatrix} 1 & sin(\phi)tan(\theta) & cos(\phi)tan(\theta) \\ 0 & cos(\phi) & -sin(\phi) \\ 0 & \frac{sin(\phi)}{cos(\theta)} & \frac{cos(\phi)}{cos(\theta)} \end{bmatrix} \cdot \begin{bmatrix} p \\ q \\ r \end{bmatrix} \tag{6}$$

At this point, it should be noted that (5) contains some uncertainties, especially about the inertia and the center of mass impacting the matrix $D(\gamma)$.

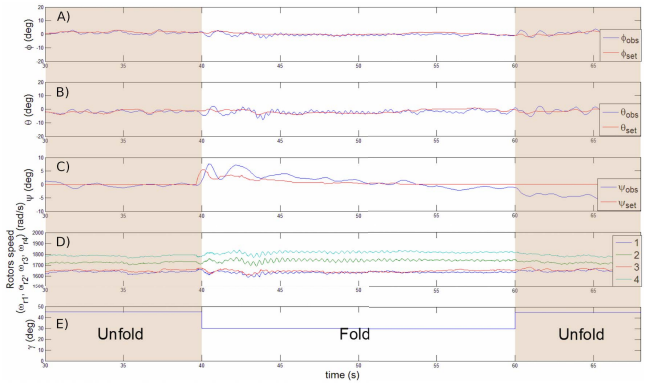

Fig. 6. **A-B-C)** Evolution of the Euler angle ϕ, θ, ψ (roll, pitch, yaw) during a folding maneuver. At time $t = 40s$, γ, half of the scissor-joint angle between the arms, is reduced by 15 deg. **D)** The evolution of Θ_{α_Y}, illustrates how the adaptive gains adapt to the new configuration. **E)** At time $t = 40s$, γ, half of the scissor-joint angle between the arms, is reduced by 15 deg and then restored at time $t = 60s$.

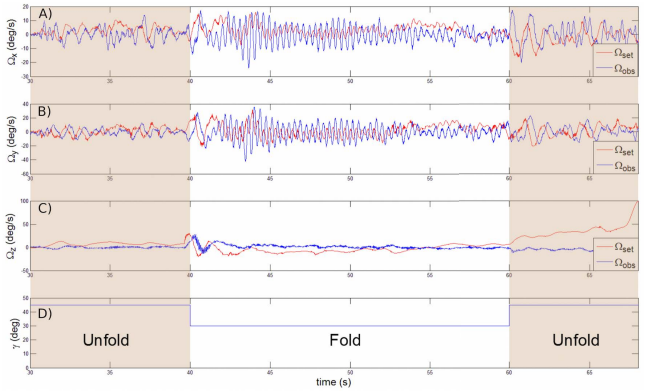

Fig. 7. **A-B-C)** The angular rate in roll, pitch, yaw during a folding maneuver. **D)** At time $t = 40s$, the disturbance occurred is major : some oscillation appears in roll and pitch. At time $t = 60s$, when the quadrotor restores its original configuration, the overshoot also is reduced while the angular rate controller is adapting to the new equilibrium point.

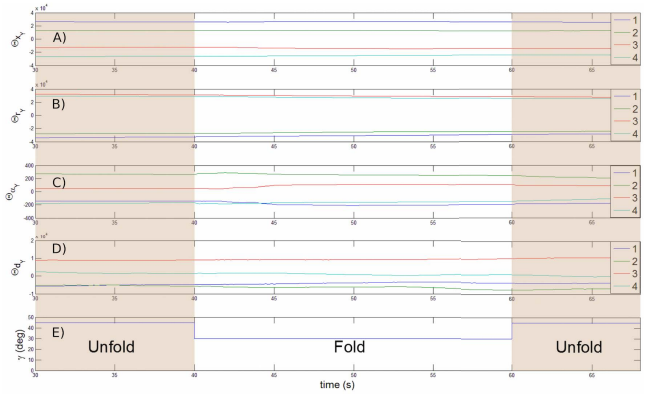

Fig. 8. **A-B-C-D)**Evolution of the four adaptive gains on the Y axis during the folding of the actuated scissor joint. Only the 4 gains on the Y axis have been presented in this figure because they exhibit the most significant variations. **E)** At time $t = 40s$, γ, half of the scissor-joint angle between the arms, is reduced by 15 deg and then restored at time $t = 60s$.

B. Control

In-flight changes in the X-geometry involve significant control challenges. Controllers are usually designed on the basis of specific previously established dynamic models which rely on a well-known geometry of a quadrotor. The center of gravity and inertias are not very easy to measure on the X-Morf aerial robot using simple experimental tech-

niques because of numerous uncertainties due to:

- the number of parts of the X-Morf, and,
- any slight displacement (or offset) in the numerous wires, electronic boards and mechanical parts such as the heavy battery.

In addition, in the case of adaptive-geometry vehicles, the dynamic model contains many time-varying parameters. A classic PID controller coupled with gain scheduling could be used to deal with the problems introduced by time varying parameters. However, tuning each gain separately would be particularly tricky, and this would not ensure that the controllers are robust enough in the case of a large variation in the X geometry. Linear Quadratic Regulator (LQR) control procedures (see [2]) could be used to tackle this issue, or adaptive control methods such as L1 adaptive control or Model Reference Adaptive Control (MRAC) methods (see [1]). The MRAC process is quite straight forward to implement and yields consistent results. In the present paper, the MRAC method was used to control the angular rate loop, which contains all the uncertainties. The attitude loop is entirely based on the exact trigonometric equation (6): a classical PID combined with a Dynamic Inversion process was used in this case to deal with the nonlinearities. The entire control architecture of the X-Morf robot is presented in Fig. 4.

1) Inner rate control loop using Adaptive control law: To implement the adaptive laws, the angular rate dynamics of the X-Morf robot has to be separated first into as many parts as there are categories of uncertainty. In the following equation (7), where $x_p = [p \quad q \quad r]$ and $u = [T_1 \quad T_2 \quad T_3 \quad T_4]$:

$$\dot{x}_p = A_p x_p + B_p u + \alpha_p h(x_p) + D.i \tag{7}$$

A_p stands for the linear dynamics and B_p stands for the response to the inputs u. α_p stands for all the non linear dynamics combined and D stands for the external disturbances, and we take $i = [111]^T$ to ensure consistency in the magnitude of the parameters. The linear part A_p can be approximately computed by performing Jacobian linearization of (5). But to identify the nonlinearities, developing the (5) yields the following nonlinear plant model:

$$\dot{x}_p = \underbrace{\mathbf{I}(\gamma)^{-1}.\mathbf{D}(\gamma)}_{B_p(\gamma)}.u - \underbrace{x_p \times (\mathbf{I}(\gamma).x_p)}_{g(x_p)} \tag{8}$$

Based on the fact that the momentums of inertia are much larger than the products of the inertia, it can be reasonably assumed that the tensor of inertia is a diagonal. Based on this assumption, we obtain (10):

$$\alpha_p(\gamma) = \begin{bmatrix} -\frac{I_z - I_y(\gamma)}{I_x(\gamma)}/ & 0 & 0 \\ 0 & -\frac{I_x(\gamma) - I_z}{I_y(\gamma)}/ & 0 \\ 0 & 0 & -\frac{I_y(\gamma) - I_x(\gamma)}{I_z} \end{bmatrix} \tag{9}$$

$$g(x_p) = \alpha_p(\gamma).\underbrace{\begin{bmatrix} r.q \\ r.p \\ p.q \end{bmatrix}}_{h(x_p)} \tag{10}$$

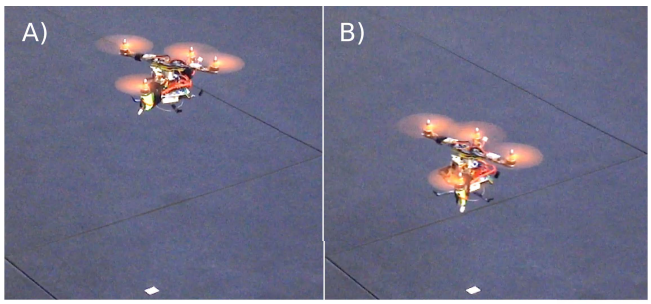

Fig. 9. In-flight changes of Quadmotor Geometry. **A)** Capture of X-Morf flying robot in unfolded position. and in folded position in **B)**. Full length video is available is supplemental material.

The control law (11) is written as follows:

$$u = \Theta_x x_p + \Theta_r \Omega_{set} + \Theta_\alpha h(x_p) + \Theta_d.i \tag{11}$$

where $\Theta_{x,r,\alpha,d}$ are the adaptive gains and i is a constant vector with the value $[111]^T$. The adaptive gains have the following architecture:

$$\Theta_j = \begin{bmatrix} \Theta_{jX_1} & \Theta_{jY_1} & \Theta_{jZ_1} \\ \Theta_{jX_2} & \Theta_{jY_2} & \Theta_{jZ_2} \\ \Theta_{jX_3} & \Theta_{jY_3} & \Theta_{jZ_3} \\ \Theta_{jX_4} & \Theta_{jY_4} & \Theta_{jZ_4} \end{bmatrix} \tag{12}$$

With $j = x, r, \alpha, d$. Note that each row corresponds to one specific rotor. For example, Θ_{rY_4} corresponds to the part of the control command driving rotor 4 in response to the angular rate command acting upon the Y axis. Applying the control law (11) to (7) gives the closed loop dynamics (13):

$$\dot{x}_p = (A_p + B_p\Theta_x)x_p + B_p\Theta_r\Omega_{set} + (B_p\Theta_\alpha + \alpha_p)h(x_p) + (B_p\Theta_d + D)i \tag{13}$$

The main idea on which the MRAC procedure is based is a question of finding the adaptive gains corresponding to convergence between the closed loop dynamics and the reference dynamics adopted, using real time methods. The reference dynamics are defined as follows (14):

$$\dot{\Omega}_{model} = A_m\Omega_{model} + B_m\Omega_{set} \tag{14}$$

where A_m and B_m describe realistic dynamics. In the present case, the reference dynamics are those of a first order filter with a convergence time of $0.1s$. By solving (13) = (14), we can obtain the optimum values of the adaptive gain. The dynamic error is defined as follows:

$$e_c = x_p - \Omega_{model} = \Omega_{obs} - \Omega_{model} \tag{15}$$

A Lyapunov based analysis gives the following adaptive laws: (16). Details of this analysis are available in [1].

$$\begin{aligned} \dot{\Theta}_x &= -\Gamma_x \hat{B}_p^T P e_c x_P^T - \sigma_x \Theta_x E_c \\ \dot{\Theta}_r &= -\Gamma_r \hat{B}_p^T P e_c \Omega_{set}^T - \sigma_r \Theta_r E_c \\ \dot{\Theta}_\alpha &= -\Gamma_\alpha \hat{B}_p^T P e_c h(x_p)^T - \sigma_\alpha \Theta_\alpha E_c \\ \dot{\Theta}_d &= -\Gamma_d \hat{B}_p^T P e_c i^T - \sigma_d \Theta_d E_c \end{aligned} \tag{16}$$

With $\hat{B}_p$ and E_c defined by (17):

$$\hat{B}_p = [\tfrac{B_{p_{ij}}}{|B_{p_{ij}}|}] \quad E_c = \begin{bmatrix} |e_x| & 0 & 0 \\ 0 & |e_y| & 0 \\ 0 & 0 & |e_z| \end{bmatrix} \tag{17}$$

The adaptation rate matrices $\Gamma_{x,r,\alpha,d}$ have to be adjusted, as do the definite positive matrix P and the damping coefficient $\sigma_{x,r,\alpha,d}$ in order to tune the adaptive gain convergence behavior.

2) Attitude loop: The attitude angles $\begin{bmatrix}\phi & \theta & \psi\end{bmatrix}$ are linked to the angular rates $\begin{bmatrix}p & q & r\end{bmatrix}$ via (6). To obtain the angular rates u_c delivered to the angular rate loop, a dynamic inversion can be used. The pseudo control is defined by:

$$v = \begin{bmatrix}\dot{\phi}_{pc} & \dot{\theta}_{pc} & \dot{\psi}_{pc}\end{bmatrix} \tag{18}$$

Since this is a linear system, it can be controlled by a classical linear controller such as a PID controller (see (19)):

$$v = (k_p + k_d s + k_i \frac{1}{s}).e \tag{19}$$

The angular rate command is then given by (20):

$$\Omega_{set} = \begin{bmatrix}1 & 0 & -sin(\theta) \\ 0 & cos(\phi) & sin(\theta).\\ 0 & -sin(\phi) & cos(\phi).cos(\theta)\end{bmatrix} v \tag{20}$$

IV. Flight test results

The adaptive rate loop controller and the PID controlling the attitude loop were first implemented in a Simulink simulator in order to test their behavior. Convergence of the adaptive gains was checked and various tunings of the PID controller were tested to obtain the required responses. With the RT-Mag toolbox, the Gumstix of the X-Morf robot was implemented very quickly, based directly on a Simulink model. The adaptive rate matrices were adjusted to ensure the stability of the adaptive law and fast convergence of the adaptive gains. To facilitate such fast convergence, adaptive rate matrices were initialized at the final values observed in the simulation. Fig. 6 shows the ability of the X-Morf robot to perform stable flight in both the unfolded and a folded configuration. In addition, Fig. 7 shows how the Adaptive angular rate control loop tracks the angular rate controlled by the attitude control loop. Fig. 9 shows the X-Morf aerial robot in both configuration (folded and unfolded) : a full length video is available in supplemental material. Fig. 8 gives an example of some relevant adaptive gains and shows how they adapt to the folding of the quadrotor. It can be seen here that only the adaptive gains Θ_{α_γ} seem to adapt to the new configuration, whereas the other adaptive gains show only some slight variations. Based on (10), the adaptive gains Θ_{α_γ} have to compensate for the α_p component of the nonlinear model: this component depends largely on the moments of inertia. Reducing the scissor-joint angle between the arms of the X-Morf robot drastically affects the inertia, and the adaptive law therefore tends to compensate for these changes by generating the appropriate adaptive gain Θ_{α_γ}. The overall angular rate and attitude tracking performances of the robot were satisfactory. The convergence of the adaptive laws can be adjusted via the angular rate matrix.

V. CONCLUSIONS

As far we know, the robot described in the present paper is the first-ever foldable quadrotor which is able to change its X-geometry during flight. The most innovative aspects of the X-Morf robot are its two arms, each equipped with two rotors, forming a scissor joint actuated by a servomotor. This reconfigurable quadrotor required a more complex control strategy than simple PIDs. The adaptive MRAC control strategy adopted has proved to be suitable for controlling the quadrotor efficiently and adaptable to its folding maneuvers. The scissor joint mechanism of future version of X-Morf robot might be simplified by decreasing its diameter by avoiding to pass the wires through its central hole. In order to develop a fully autonomous quadrotor, we intend to equip the X-Morf robot in the near future with sensors such as micro-cameras or LIDAR devices so that it will be able to detect any narrowing of the flight path ahead and adapt its span accordingly on the fly.

ACKNOWLEDGMENT

The authors would like to thank N. Marchand, A. Manecy, F. Colonnier and E. Vanhoutte for their helpful comments and suggestions during this research and J. Blanc for improving the English manuscript.

References

[1] Achtelik, M., Bierling, T., Wang, J., Höcht, L., Holzapfel, F.: Adaptive Control of a Quadcopter in the Presence of large/complete Parameter Uncertainties. American Institute of Aeronautics and Astronautics (2011)

[2] Argentim, L.M., Rezende, W.C., Santos, P.E., Aguiar, R.A.: Pid, lqr and lqr-pid on a quadcopter platform. In: Informatics, Electronics Vision (ICIEV), 2013 International Conference on, pp. 1–6 (2013)

[3] Daler, L., Mintchev, S., Stefanini, C., Floreano, D.: A bioinspired multi-modal flying and walking robot. Bioinspiration and Biomimetics **10**(1), 016,005 (2015)

[4] Grant, D.T., Abdulrahim, M., Lind, R.: Design and analysis of biomimetic joints for morphing of micro air vehicles. Bioinspiration and Biomimetics **5**(4), 045,007 (2010)

[5] Heredia, G., Duran, A., Ollero, A.: Modeling and simulation of the hada reconfigurable uav. Journal of Intelligent & Robotic Systems **65**(1), 115–122 (2012)

[6] Landry, B., Deits, R., Florence, P.R., Tedrake, R.: Aggressive quadrotor flight through cluttered environments using mixed integer programming. In: 2016 IEEE International Conference on Robotics and Automation (ICRA), Stockhom, Sweden (2016)

[7] Lee, J., Oh, S., Yee, K., Kim, D.K.: Numerical investigation on overlap effects of tandem rotors in forward flight. International Journal of Aeronautical and Space Sciences **10**(2), 63–76 (2009)

[8] Mahony, R., Hamel, T., Pflimlin, J.M.: Nonlinear complementary filters on the special orthogonal group. IEEE Transactions on Automatic Control **53**(5), 1203–1218 (2008)

[9] Manecy, A., Marchand, N., Ruffier, F., Viollet, S.: X4-mag: A low-cost open-source micro-quadrotor and its linux-based controller. International Journal of Micro Air Vehicles **7**(2), 89–109 (2015)

[10] Mellinger, D., Michael, N., Kumar, V.: Trajectory generation and control for precise aggressive maneuvers with quadrotors. The International Journal of Robotics Research **31**(5), 664–674 (2012)

[11] Mestrinho, J., Gamboa, P., Santos, P.: Design Optimization of a Variable-Span Morphing Wing for a Small UAV. American Institute of Aeronautics and Astronautics (2011)

[12] Mintchev, S., Daler, L., L'Eplattenier, G., Saint-Raymond, L., Floreano, D.: Foldable and self-deployable pocket sized quadrotor. In: 2015 IEEE International Conference on Robotics and Automation (ICRA), pp. 2190–2195 (2015)

[13] Otsuka, H., Nagatani, K.: Thrust loss saving design of overlapping rotor arrangement on small multirotor unmanned aerial vehicles. In: 2016 IEEE International Conference on Robotics and Automation (ICRA), Stockhom, Sweden, pp. 3242–3248 (2016)

[14] Schiffner, I., Vo, H.D., Bhagavatula, P.S., Srinivasan, M.V.: Minding the gap: in-flight body awareness in birds. Frontiers in Zoology **11**(1), 1–9 (2014)

[15] Stowers, A.K., Lentink, D.: Folding in and out: passive morphing in flapping wings. Bioinspiration and Biomimetics **10**(2), 025,001 (2015)